

Massage Acupoint Positioning Method of Human Body Images Based on Transfer Learning

Chao Zhang¹, Qian Wu¹, Ju Wang¹, Liyan Yang², Hongxia Zhang^{3*}

¹ Electronic Information Engineering College, Changchun University, Changchun 130000, China

² Datang Jilin Power Generation Co., Ltd. Changchun Third Thermoelectric Branch, Changchun 130000, China

³ Rehabilitation Hospital of China-Japan Union Hospital, Changchun 30000, China

Corresponding Author Email: zhx321122@jlu.edu.cn

Copyright: ©2023 IETA. This article is published by IETA and is licensed under the CC BY 4.0 license (<http://creativecommons.org/licenses/by/4.0/>).

<https://doi.org/10.18280/ts.400636>

ABSTRACT

Received: 5 June 2023

Revised: 26 September 2023

Accepted: 20 October 2023

Available online: 30 December 2023

Keywords:

transfer learning, human body images, massage acupoints, acupoint positioning

Traditional Chinese massage therapy is a very popular method to stay healthy, which regulates body balance, alleviates fatigue, and prevents diseases by massaging specific acupoints. Although computer vision has been increasingly applied in traditional Chinese medicine, related study of acupoint positioning is still insufficient. The existing acupoint positioning methods mainly rely on manual labeling and rule matching, which often require a large amount of manual intervention with limited accuracy. Therefore, this study proposed a massage acupoint positioning method of human body images based on transfer learning. The massage acupoint meridian and collateral positioning principle of human body images was presented. Using the integrated deep belief network model as a pre-trained model, a feasible transfer learning model was established through fine-tuning and feature mapping. The experimental results verified that the proposed method was effective. Relevant research results provide useful references for research in related fields.

1. INTRODUCTION

With the accelerated pace of life and the increasing life pressure, more and more people have started to pay attention to physical health and healthcare. Traditional Chinese massage therapy is a very popular healthcare method, which regulates body balance, alleviates fatigue, and prevents diseases by massaging specific acupoints [1]. However, the acupoint positioning accuracy is crucial for the massage effect, and acupoint positioning is a challenging task [2]. Therefore, it is of important practical application value to study an automatic acupoint positioning method of human body images based on computer vision [3-5].

In the past few years, significant progress has been made in the research field of computer vision, especially image recognition, segmentation, and processing. A major breakthrough has been made in deep learning technology, especially convolutional neural network (CNN) [6-9], in this regard. As an effective learning strategy, transfer learning allows a pre-trained model to be applied to new tasks, thus improving the generalization ability and accuracy of the model [10].

Computer vision and deep learning have made significant progress in many fields in the past few years, including object detection [11-14], face recognition [15-19], and pose estimation [20-23]. These successful applications provide insights for the research in other fields. Although computer vision has made some progress in the application of traditional Chinese medicine [24], the research on acupoint positioning is

still insufficient. The acupoint positioning accuracy is crucial for the effect of massage therapy. Therefore, it is of great value to find an efficient and reliable computer vision method to solve this problem.

The existing acupoint positioning methods mainly rely on manual labeling and rule matching [25], which often require a large amount of manual intervention with limited accuracy. In order to overcome these problems, a massage acupoint positioning method of human body images based on transfer learning was proposed in this study. Transfer learning allows to use pre-trained deep neural networks, such as VGG-16 [26], or deep residual network (ResNet) [27], to achieve high positioning precision on a limited labeled dataset. In addition, training time and consumption of computing resources can also be reduced by applying transfer learning to acupoint positioning tasks [28].

This study proposed a massage acupoint positioning method of human body images based on transfer learning. Relevant work was introduced in Section 2, including the massage acupoint meridian and collateral positioning principle of human body images. Using the integrated deep belief network (DBN) model as a pre-trained model, a feasible transfer learning model was established through fine-tuning and feature mapping. This process was described in detail in Section 3. Experimental results and analysis were reported in Section 4. Contributions of this study were summarized, and pertinent future research directions were discussed in Section 5.

2. MESSAGE ACUPOINT MERIDIAN AND COLLATERAL POSITIONING PRINCIPLE OF HUMAN BODY IMAGES

The input unknown human back image was pre-processed first, such as adjusting the size, contrast, and brightness of the image, in order to adapt to the subsequent processing process. Human pose estimation was performed for the input image, which extracted the coordinates of key human body points, such as spine, shoulders, etc. These key points served as reference points to help identify the region of interest (ROI). Then the prior meridian and collateral model was mapped to the image to be detected, which was achieved by transforming and scaling the coordinates of key points. In the mapped meridian and collateral model, the positions of specific massage acupoints were found, and a ROI was created around them. This region was a rectangular box or circular region, and its size was adjusted according to the actual situation. It helped focus on the parts of the image related to specific acupoints, thus reducing computational complexity and improving accuracy. Specific massage acupoints were identified within the generated ROI. The model learned and recognized the acupoint features according to training data. Through the above steps, the prior meridian and collateral model was used to automatically establish the ROI for specific massage acupoints in the human back image to be detected, and identify the accurate acupoint positions.

Based on the ROI establishment, the Dijkstra algorithm was further replaced with the Fast Marching Method (FMM) for massage acupoint meridian and collateral positioning. The FMM eigenfunction was adjusted based on prior information, which aimed to guide the algorithm in considering specific constraints and preferences when searching for the shortest path. For example, prior information of the meridian and collateral model was encoded into the eigenfunction to optimize the algorithm performance. Compared with Dijkstra algorithm, the FMM had significant advantages in computation speed, especially when processing large-scale image data. The FMM used numerical simulation methods to solve the eikonal equation, which found the shortest path more effectively. Therefore, massage acupoint meridian and collateral positioning of human images was effectively achieved by introducing the prior information provided by the prior model into the FMM eigenfunction. Figure 1 shows the FMM point set classification diagram.

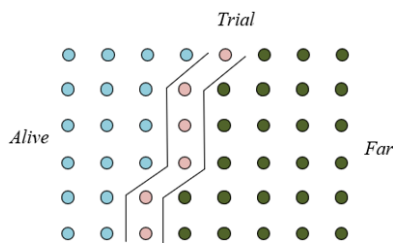


Figure 1. Classification diagram of the FMM point set

The FMM is used to solve the eikonal equation, which has been widely used in application scenarios of medical image processing and linear feature positioning. The eikonal equation is a kind of nonlinear partial differential equation. Let s be the position, $U(s)$ be the velocity function of wave propagation at the current position, $G(s)$ be the time function to reach the current position, and ∇G be the gradient of the time function, then the formula was:

$$U(s)|\nabla G(s)|=1 \quad (1)$$

To obtain the discrete solution of the eikonal equation, a discrete grid was used for spatial mapping in three-dimensional space. Let a , b and c be the components of different coordinate axes of the 3D discrete grid; $k(s_a, r_b, q_c)$ be the corresponding point in the real world; Δs , Δr and Δq be the distances on the coordinate axes x , y and z , respectively. The gradient $\nabla G(s)$ was discretized as follows:

$$\begin{aligned} & \max(W_{abc}^{-s}G, 0)^2 + \max(W_{abc}^{+s}G, 0)^2 + \max(W_{abc}^{-r}G, 0)^2 \\ & + \max(W_{abc}^{+r}G, 0)^2 + \max(W_{abc}^{-q}G, 0)^2 \\ & + \min(W_{abc}^{+q}G, 0)^2 = \frac{1}{U_{abc}^2} \end{aligned} \quad (2)$$

where,

$$W_{abc}^{-s} = \frac{G_{a,b,c} - G_{a-1,b,c}}{\Delta s}, W_{abc}^{+s} = \frac{G_{a+1,b,c} - G_{a,b,c}}{\Delta s} \quad (3)$$

$$W_{abc}^{-r} = \frac{G_{a,b,c} - G_{a,b-1,c}}{\Delta r}, W_{abc}^{+r} = \frac{G_{a,b+1,c} - G_{a,b,c}}{\Delta r} \quad (4)$$

$$W_{abc}^{-q} = \frac{G_{a,b,c} - G_{a,b-1,c}}{\Delta q}, W_{abc}^{+q} = \frac{G_{a,b+1,c} - G_{a,b,c}}{\Delta q} \quad (5)$$

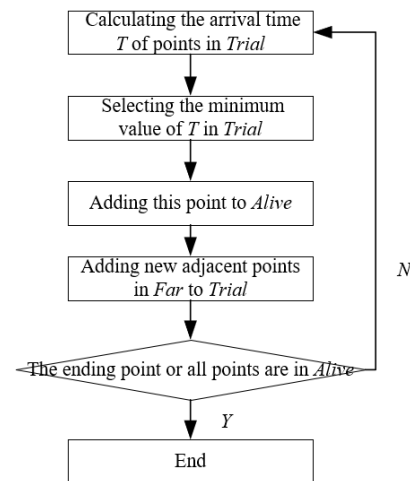


Figure 2. FMM flow chart

The FMM was used for massage acupoint meridian and collateral path positioning on the back of the human body. First, the ROI was automatically established in the unknown human back image to be detected, which was achieved by preprocessing images, estimating human poses, mapping prior models, and other methods, aiming to determine the approximate position range of specific massage acupoints. Second, the prior information provided by the meridians and collaterals of the prior model was added to the massage acupoint meridian and collateral features of the human back, which helped the FMM find the correct meridian and collateral path in the image more accurately. Third, prior information was introduced into the eikonal equation, which enabled the FMM to consider the prior information when searching for the shortest path. The eikonal equation described the cost function,

which represented the connection strength between points on the meridian and collateral path. The starting and ending points within the ROI were manually labeled. These two points represented the starting and ending positions of the meridian and collateral path, usually corresponding to specific massage acupoints. Finally, forward propagation was carried out throughout the entire ROI, which gradually progressed along the minimum cost path from the starting point to the ending point. Based on numerical simulation, the FMM was used to solve eikonal equation to effectively find the shortest path. Figure 2 shows the FMM flow chart.

Energy model V was constructed. Let K be the feature of the current position. A constant ζ needed to be introduced to make the expression greater than 0, because the value of K near the massage acupoint meridian and collateral center was smaller. The path with the smallest integral in $K=K+\zeta$ was searched, which transformed the massage acupoint meridian and collateral positioning on the back of the human body into the problem of finding the global minimum value. Let $X(g)$ be the curve on the massage acupoint meridian and collateral image, Ψ be the curve length, and $[0,L][0,O]$ be the domain of definition, then there were:

$$V(X) = \int_{\Psi} (K(X(g)) + \zeta) dg \quad (6)$$

Let Ω_{s-e} be the set of all paths between the starting and ending points of massage acupoint meridians and collaterals of the human back, and F be the energy integral value of the minimum path between the meridian and collateral starting point and any point in the ROI. To obtain the minimum path energy integral value for each point in the ROI, it was necessary to propagate forward from the starting point, with K always greater than 0 during the propagation process. Let K_s and K_e be the starting and ending points of the F -measure graph, respectively. It was considered that the unique local minimum value was obtained at K_s , satisfying $F(k_s)=0$. To obtain the minimum integration path from K_s to K_e , the backpropagation from K_e to K_s on the F -measure graph was needed only.

$$F(k) = \inf_{Ap} E(X) = \inf_{Ap} \left\{ \int_{\Omega} \tilde{K}(X(g)) dg \right\} \quad (7)$$

Let (a,b,c) be each voxel in the back image of the human body, then the F -measure of (a,b,c) and its six surrounding neighboring voxels needed to meet the following formula:

$$\begin{aligned} & \left(\max \{ f - F_{a-1,b,c}, u - F_{a+1,b,c}, 0 \} \right)^2 + \\ & \left(\max \{ f - F_{a,b-1,c}, u - F_{a,b+1,c}, 0 \} \right)^2 + \\ & \left(\max \{ f - F_{a,b,c-1}, u - F_{a,b,c+1}, 0 \} \right)^2 = \tilde{K}_{a,b,c}^2 \end{aligned} \quad (8)$$

For the model registration massage acupoint meridian and collateral positioning algorithm proposed in this study, it integrated prior information provided by the ROI of massage acupoint meridians and collaterals. Figure 3 shows the comparison of meridian and collateral positioning at interference points. For the massage acupoint meridians and collaterals, let $l(c)$ be the inertia feature, $s(c)$ be the voxel feature, and $g(c)$ be the enhancement, then the eigenfunction mainly included features in these three aspects. The parameter

o was set to prevent the denominator from being zero. Let δ , ϖ and λ be the indexes of $l(c)$, $s(c)$ and $g(c)$, respectively, then the definition equation of the eigenfunction was as follows:

$$K(c) = \frac{1}{l(c)^\delta * s(c)^\varpi * g(c)^\lambda + \varepsilon} \quad (9)$$

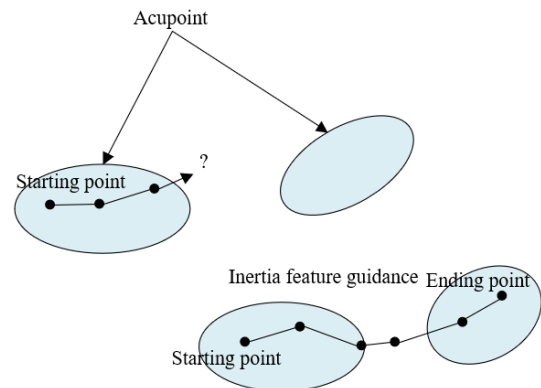


Figure 3. Meridian and collateral positioning comparison at interference points

Inertia feature was used for guidance in the process of tracking meridians and collaterals in this study. After obtaining the inertia feature of the massage acupoint meridians and collaterals through the meridian and collateral model in the prior model, the meridian and collateral model and positioning results were divided into multiple segments with the same length for processing, which better adapted to meridians and collaterals with different lengths, and improved the positioning accuracy. The starting and ending points of the meridian and collateral model were defined as the points closest to the starting and ending points of the blood vessel to be positioned, which aimed to ensure that the positioning process always centered around the blood vessel. An eigenfunction without inertia feature was used for the first-segment positioning of meridians and collaterals in the unknown image to be detected, because there was not enough information to introduce the inertia feature during the first-segment positioning. At the same time, to fully utilize the inertia feature and improve the positioning effect, the corresponding meridian and collateral model was mapped to the previous-segment positioning results of the meridians and collaterals, and the same mapping was applied to the current-segment meridian and collateral model.

Let $w(c)$ be the distance between the current position and the current-segment starting point during the massage acupoint meridian and collateral positioning process, αw be the distance between the guidance position of the mapped meridian and collateral model and the current-segment starting point, and βw be the distance standardization parameter, then there were:

$$l(c) = e^{-\frac{1}{2} \left(\frac{w(c) - \alpha w}{\beta w} \right)^2} \quad (10)$$

Let $j(c)$ be the current value of voxel grayscale at a given position, and α_j be the average voxel grayscale in the entire ROI. Based on the gray value features of voxels at various positions in the ROI of the unknown human back image, the voxel feature $s(c)$ of the massage acupoint meridians and collaterals was further defined as follows:

$$s(c) = e^{-\frac{1}{2}(j(c)-\alpha_j)^2} \quad (11)$$

For the above model registration algorithm for massage acupoint meridian and collateral positioning of the human back, the meridian and collateral model from the prior model was introduced, which obtained prior knowledge about the structures and shapes of meridians and collaterals. This helped provide more accurate guidance during the positioning process, thus improving the accuracy of the positioning results. At the same time, the meridian and collateral model and positioning results were divided into multiple segments with the same length for processing, which better adapted to meridians and collaterals with different lengths, and improved the positioning accuracy.

3. TRANSFER PLAN

Existing models may perform well on training datasets, but did not adapt well to different individuals and scenarios in practical applications, because significant differences in the shapes and positions of massage acupoints on the back of the human body led to insufficient generalization ability of the models. At the same time, the training data for the human back massage acupoint positioning may be limited in quantity or unevenly distributed in practical applications, which resulted in the models not being able to fully learn the features of various samples during the training process, thus affecting their performance in actual scenarios.

Transfer learning used the knowledge of pre-trained models, such as models obtained through training on large-scale datasets, to transfer the knowledge to new tasks, which avoided training the models from scratch, thus reducing training time and computational resource consumption. The integrated DBN model was used as the pre-trained model, and a feasible transfer learning model was established through fine-tuning and feature mapping. The DBN was a deep model that learned complex feature representations of data. When the DBN was used as a pre-trained model, its advantages in feature extraction were fully utilized, which provided richer feature representations for new tasks. A new network structure was built, by setting parameters of different layers in the network as "frozen", "fine-tuned" or not, or by adding the "adaptive layer" or not, to adapt to different task needs, which provided more possibilities to solve the difference problem of various scenarios and individuals. Figure 4 shows the model framework based on deep transfer learning.

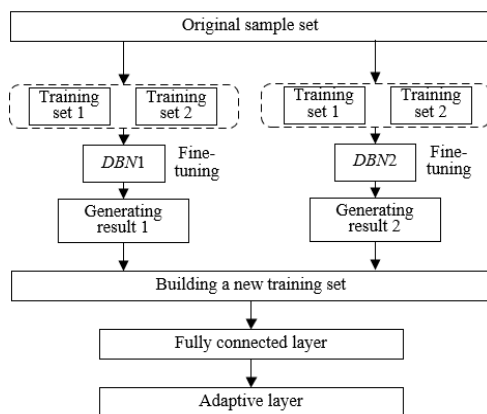


Figure 4. Model based on deep transfer learning

In the transfer learning task, differences often exist in the data distributions between the source and target domains, leading to the problem of domain drift. Adding an adaptive layer and adopting the multiple kernel-maximum mean discrepancy (MK-MMD) method effectively measured the distribution differences between both domains, thus alleviating the domain shift problem. The MK-MMD combined the multi-kernel idea, which was used for a weighted combination of MMD under different kernel functions, enabling the MK-MMD to have stronger representation capabilities and capture more complex distribution differences between the source and target domains. The $\omega(\cdot)$ function was introduced to calculate the maximum mean difference between data distributions h and f in two different domains based on the following formula:

$$MMD^2(h, f) = \sup_{\omega|_S \leq 1} \left\| V_{c^h \sim h} [\omega(c^h)] - V_{c^f \sim f} [\omega(c^f)] \right\|_S^2 \quad (12)$$

Let $V_{x^h \sim h}[\cdot]$ be the mathematical expectation of the data distribution in the source domain, $|\omega|_S \leq 1$ be a series of functions in the unit ball in the reproducing kernel Hilbert space (RKHS), and $W_H = \{C^h_i\}_{i=1}^n = 1$ and $W_F = \{C^f_i\}_{i=1}^n = 1$ be the sample sets in distributions h and f . The following equation provided the empirical estimation formula expression of the MMD:

$$MMD^2(W_H, W_F) = \left\| \frac{1}{N} \sum_{i=1}^n \omega(c^h_i) - \frac{1}{M} \sum_{j=1}^n \omega(c^f_j) \right\|_S^2 \quad (13)$$

Let $\omega(\cdot)$ be the feature mapping concerning the kernel mapping $p(c^h, c^f) = \langle \omega(c^h), \omega(c^f) \rangle$, then the convex combination of O basic cores $p_o(c^h, c^f)$ was $p(c^h, c^f)$:

$$p(c^h, c^f) = \sum_{o=1}^O \gamma_o p_o(c^h, c^f), \quad s.t. \gamma_o \geq 0, \sum_{o=1}^O \gamma_o = 1 \quad (14)$$

To achieve better effect, this study optimized the main MMD method using a single-state kernel, i.e. adopted a strategy of multiple kernel linear combinations.

In the RKHS S_p with the unique kernel p , let independent element $\gamma_p(k)$ be the mean value of distribution k , then $V_{c \sim k} u(c) = \langle u(c), \gamma_p(k) \rangle_{S_p}$, with $u \in (S_k)$. In S_k , let MK-MMD $w_p(k, j)$ be the mean distance of distributions k and j , then its square formula was as follows:

$$w_p^2(k, j) = \left\| V_k [\omega(x^h)] - V_j [\omega(x^f)] \right\|_S^2 \quad (15)$$

Same as the maximum mean difference, feature mapping ω was associated with the unique kernel, i.e., $p(c^h, c^f) = \langle \omega(c^h), \omega(c^f) \rangle$. $p(c^h, c^f)$ was defined as a convex combination of n PSD kernels $\{p_u\}$: $P\Delta = \{p = \sum_{i=1}^n \gamma_i p_i; \sum_{i=1}^n \gamma_i = 1, \gamma_i \geq 0, \forall i\}$, with relevant constraints of coefficient cage $\{\gamma_i\}$ guaranteeing to generate the unique multi-kernel $p^{\#1}$.

Figure 5 shows the improved network model structure diagram. Different kernel functions have different feature capture capabilities and scales. By combining multiple kernel functions, the MK-MMD better captured the feature differences between the source and target domains at different scales, thus improving the model's performance in the transfer

learning task. Meanwhile, the diversity of kernel combination schemes enabled the MK-MMD to have stronger generalization ability. The optimal kernel selection scheme may vary under different tasks and data distributions. The model better adapted to different scenarios by finding the optimal kernel selection scheme.

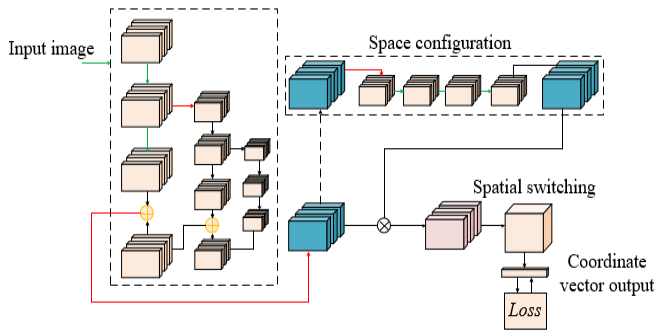


Figure 5. Structure diagram of improved network model

4. EXPERIMENTAL RESULTS AND ANALYSIS

Samples used for massage acupoint positioning of human body images were divided into three categories. The first category was the normal acupoint samples, including normal massage acupoint images of human bodies with clearly visible acupoints, which were used to train and validate the models, thus enabling them to learn to recognize and locate acupoints under normal conditions. The second category was the abnormal acupoint samples, including massage acupoint images with abnormal or pathological conditions, such as injuries, redness, swelling, and inflammation in the acupoints, which were used to train and validate the models, thus helping them identify and process abnormal acupoint situations in practical applications. The third category was the background interference samples, mainly including background areas

unrelated to acupoints, such as clothing, skin texture, instruments, etc., which were used to train and validate the models, and help them learn to recognize and locate massage acupoints in complex backgrounds, thus improving the robustness of the models.

Performance of different network models on normal acupoint samples could be analyzed according to Table 1. It can be seen from the table that the model in this study performs well in all indexes. Compared with random forest, ResNet, and U-Net models, the model in this study has the lowest median (1.251) and mean (1.625), and lower variance (0.539), indicating that the model's prediction results have high precision and stability. At the same time, the model has the highest accuracy (102%), indicating that the model can accurately locate acupoints. In addition, the model has 4.11 seconds of predicted time, which means a faster prediction speed compared with other models. The model is superior, mainly because it used MK-MMD as an adaptive measurement method, which effectively measured the distribution differences between the source and target domains, thus alleviating the domain shift problem and improving the model's adaptability. At the same time, the optimal kernel combination scheme was selected to enhance the effect of MK-MMD, which improved the model's performance.

Performance of different network models in evaluating abnormal acupoint samples could be analyzed according to Table 2. Similar to the previous conclusion, the model in this study performs well in various indexes. The model has 2.658 median, 2.041 mean, and 0.629 variance, indicating that the model's prediction results have high precision and stability. Meanwhile, the model has a high accuracy (82.61%), indicating that the model can accurately locate abnormal acupoints. The predicted time is 2.46 seconds, which means that this model has a faster prediction speed compared with other models. The main reasons were that the model appropriately balanced and processed abnormal acupoint samples during the training process, and appropriate network structure and adaptive method were adopted.

Table 1. Evaluation results of normal acupoint samples

Network Models	Median	Mean	Variance	Accuracy (%)	Predicted Time (s)
Model in this study	1.251	1.625	0.539	102	4.11
Random forest	2.958	2.958	1.041	85.62	5.69
ResNet	5.041	5.037	1.958	11.96	4.38
U-Net	2.574	2.114	0.579	35.82	5.13

Table 2. Evaluation results of abnormal acupoint samples

Network Models	Median	Mean	Variance	Accuracy (%)	Predicted Time (s)
Model in this study	2.658	2.041	0.629	82.61	2.46
Random forest	2.15	3.629	1.352	53.48	6.18
ResNet	5.614	6.528	1.748	15.92	4.35
U-Net	3.592	3.417	0.821	42.58	5.02

Table 3. Evaluation results of background interference samples

Network Models	Median	Mean	Variance	Accuracy (%)	Predicted Time (s)
Model in this study	1.258	2.417	0.638	92.37	5.38
Random forest	2.301	2.605	1.274	61.57	6.02
ResNet	5.629	5.392	1.305	13.62	4.19
U-Net	3.457	3.514	0.629	42.59	5.38

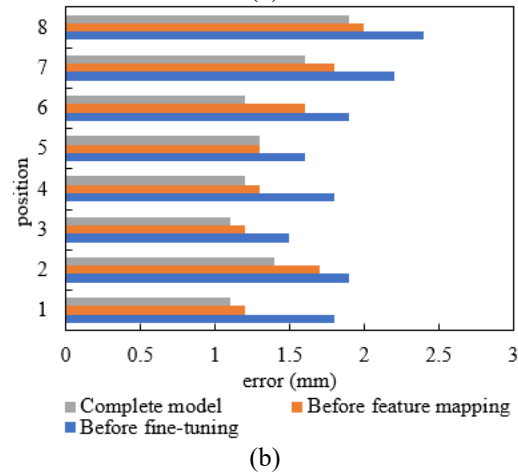
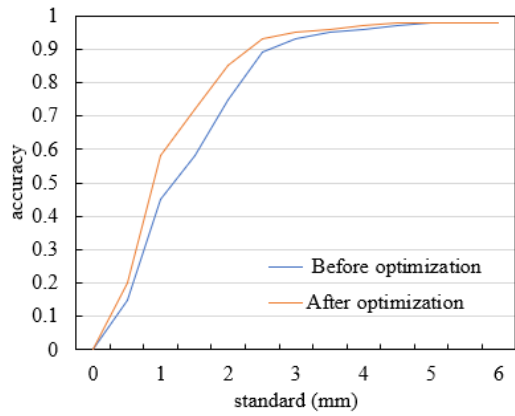


Figure 6. Comparison of accuracy curves and positioning effect in different regions

Performance of different network models in evaluating background interference samples could be analyzed according to Table 3. The model in this study performs well in various indexes. The median, mean and variance are 1.258, 2.417, and 0.638, respectively, indicating that the model's prediction results have high accuracy and stability. At the same time, the model has the highest accuracy (92.37%), indicating that the model can accurately locate acupoints in background interference samples. The predicted time is 5.38 seconds, which is the same as that of U-Net, but has better performance. The main reasons were that the model appropriately processed background interference samples during the training process, and appropriate network structure and adaptive method were adopted.

Figure 6 shows the comparison of accuracy curves and positioning effect in different regions. According to Figure 6(a), it can be seen that the positioning accuracy of the model before optimization increases with the increase of the standard. In the low standard (0-2mm) range, the accuracy is relatively low, ranging from 0 to 0.45. In the medium standard (3-5mm) range, there is a significant improvement in accuracy, ranging from 0.58 to 0.89. In the high standard (6mm and above) range, the accuracy further improves, reaching a range of 0.93 to 0.98. The optimized model has improved positioning accuracy under various standards. In the low standard (0-2mm) range, the accuracy increases from 0.2 to 0.58. In the medium standard (3-5mm) range, the accuracy improves to 0.72-0.93. In the high standard (6mm and above) range, the accuracy remains at a relatively high level, ranging from 0.95 to 0.98. By comparing the models before and after optimization, it can be seen that the positioning accuracy of the optimized model

has improved under various standards, and the improvement is more significant especially in the low and medium standard ranges, indicating that the optimized model has better performance in terms of positioning precision and stability, mainly because more suitable network structure and parameter setting were adopted in this study to achieve better feature extraction and generalization capabilities.

According to Figure 6(b), it can be observed that the positioning error range of the model at each acupoint before fine-tuning is between 1.5-2.4. Overall, the positioning precision of the model in all acupoints is acceptable, but there is still room for improvement. The positioning error range of the model before feature mapping is between 1.2-2.0. Compared with the model before fine-tuning, the positioning error of each acupoint has reduced, and the reduction is more significant especially in Acupoints 6, 7, and 8. After completing all optimization operations, the positioning error range of the model at each acupoint is between 1.1-1.9. Compared with the model before feature mapping, the positioning error of each acupoint is further reduced, and the reduction is more significant especially in Acupoints 1, 2, 3, and 6. The main reason why the optimized model had advantages was that the pre-trained model was fine-tuned, which better adapted to the characteristics of acupoint positioning tasks, thus improving the positioning precision. At the same time, the model may have adopted more effective feature extraction and fusion strategies in the feature mapping stage, which helped enhance the model's ability in recognizing acupoint features.

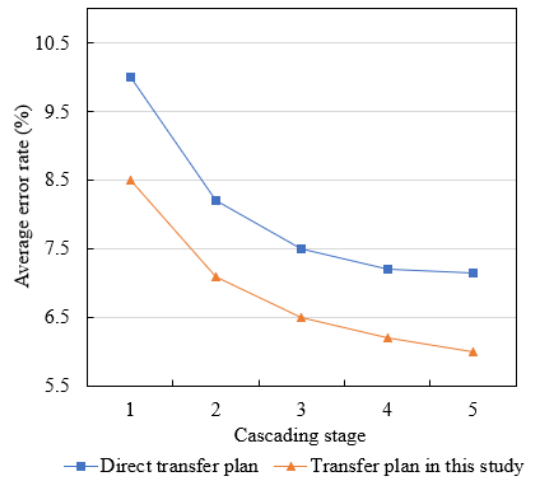


Figure 7. Average error rate of acupoint positioning using different transfer methods

According to Figure 7, the average error rates of acupoint positioning in different cascading stages using different transfer methods (direct transfer plan and the transfer plan in this study) can be observed. As shown in the figure, the average error rate of each cascading stage gradually decreases in the direct transfer plan, reducing from 10 in the first stage to 7.15 in the fifth stage. Overall, the positioning precision improves with the increase of cascading stage. In the transfer plan in this study, the average error rate of each cascading stage also shows a gradually decreasing trend, reducing from 8.5 in the first stage to 6 in the fifth stage. Compared with the direct transfer plan, the average error rate of the transfer plan in this study is lower at all cascading stages. By comparing different transfer methods, it can be seen that the average error rate of acupoint positioning in the transfer plan in this study is

lower than that in the direct transfer plan at all cascading stages, indicating that the transfer plan in this study has certain advantages in improving the acupoint positioning precision and exhibits better performance.

5. CONCLUSION

A massage acupoint positioning method of human body images based on transfer learning was proposed in this study. The massage acupoint meridian and collateral positioning principle was presented. Using the integrated DBN model as a pre-trained model, a feasible transfer learning model was established through fine-tuning and feature mapping. This study aimed to improve the performance of the model in acupoint positioning tasks. The acupoint positioning precision was improved and the positioning error was reduced in this study successfully through fine-tuning and feature mapping of the model, optimization of cascading stages, and use of different transfer plans. Combined with the above analysis, the conclusions of this study were summarized in the following aspects:

1. Model optimization. This study reduced the positioning error and improved the positioning precision at different acupoints through fine-tuning and feature mapping of the model, and optimization of the complete model, indicating that the optimization strategy adopted in this study was effective in improving the model's performance.

2. Positioning accuracy of different standards. The optimized model exhibited superior positioning accuracy in each standard, and the improvement was more significant especially in the low and medium standard ranges, indicating that the optimized model had better performance in terms of positioning precision and stability.

3. Transfer plan. Compared with the direct transfer plan, the transfer plan proposed in this study had a lower average error rate and better performance in acupoint positioning tasks, indicating that the transfer plan proposed in this study had certain advantages and application value in improving the acupoint positioning precision.

In summary, this study successfully improved the acupoint positioning precision and reduced the positioning error through model optimization, positioning accuracy analysis of different standards, and comparison of transfer plans. The method proposed in this study has certain advantages and application value in acupoint positioning tasks, providing useful references for research in related fields.

ACKNOWLEDGMENTS

This work was supported by the project of Jilin Provincial Science and Technology Department (Grant No: 20230204096YY and 20230101233JC), the Project of Jilin Provincial Development and Reform Commission (Grant No: 2023C042-4) and the project of Jilin Province Education Department (Grant No: JJKH20230672KJ).

REFERENCES

[1] Yu, W., Ma, M., Chen, X., Min, J., Li, L., Zheng, Y., Li, Y., Wang, J., Wang, Q. (2017). Traditional Chinese medicine and constitutional medicine in China, Japan

and Korea: A comparative study. *The American Journal of Chinese Medicine*, 45(1): 1-12. <https://doi.org/10.1142/S0192415X1750001X>

[2] Zhang, C., Yu, L., Hu, X.Q., Wu, Q., Wang, J., Xu, Z. (2023). A novel visual positioning algorithm for massage acupoints based on image registration. *Traitement du Signal*, 40(2): 567-575. <https://doi.org/10.18280/ts.400215>

[3] Su, M.T., Chiang, M.L., Tsai, C.H., Lin, C.W., Liu, R.X., Juang, Y.T., Chen, H.H. (2023). An acupoint health care system with real-time acupoint localization and visualization in augmented reality. *Multimedia Systems*, 29: 2217-2238. <https://doi.org/10.1007/s00530-023-01104-y>

[4] Jia, Y.K., Ding, R.T., Ren, W., Shu, J.F., Jin, A.X. (2021). Gesture recognition of somatosensory interactive acupoint massage based on image feature deep learning model. *Traitement du Signal*, 38(3): 565-572. <https://doi.org/10.18280/ts.380304>

[5] Shu, J.F., Ding, R.T., Jin, A.X., Zhu, H., Chen, S. (2022). Acupoint selection for autonomous massage based on infrared thermography. *Traitement du Signal*, 39(1): 355-362. <https://doi.org/10.18280/ts.390137>

[6] Ding, X.Y., Hu, W.J. (2023). Advancements in geological disaster monitoring and early warning systems: A deep learning and computer vision approach. *Traitement du Signal*, 40(3): 1195-1202. <https://doi.org/10.18280/ts.400336>

[7] Othman, N.A., Aydin, I. (2022). A new UAV-based social distance detector for COVID-19 outbreaks reduction, using IoT, computer vision and deep learning technologies. *Traitement du Signal*, 39(6): 1951-1959. <https://doi.org/10.18280/ts.390607>

[8] Mukkapati, N., Anbarasi, M.S. (2022). Brain tumor classification based on enhanced CNN model. *Revue d'Intelligence Artificielle*, 36(1): 125-130. <https://doi.org/10.18280/ria.360114>

[9] Palakodati, S.S.S., Chirra, V.R., Dasari, Y., Bulla, S. (2020). Fresh and rotten fruits classification using CNN and transfer learning. *Revue d'Intelligence Artificielle*, 34(5): 617-622. <https://doi.org/10.18280/ria.340512>

[10] Pan, S.J., Yang, Q. (2009). A survey on transfer learning. *IEEE Transactions on Knowledge and Data Engineering*, 22(10): 1345-1359. <https://doi.org/10.1109/TKDE.2009.191>

[11] Girshick, R., Donahue, J., Darrell, T., Malik, J. (2015). Region-based convolutional networks for accurate object detection and segmentation. *IEEE Transactions on Pattern Analysis and Machine Intelligence*, 38(1): 142-158. <https://doi.org/10.1109/TPAMI.2015.2437384>

[12] Wu, Y., Kirillov, A., Massa, F., Lo, W.Y., Girshick, R. (2020). Detectron2: A pytorch-based modular object detection library. *arXiv preprint arXiv:2006.03649*.

[13] Bochkovskiy, A., Wang, C.Y., Liao, H.Y.M. (2020). Yolov4: Optimal speed and accuracy of object detection. *arXiv preprint arXiv:2004.10934*.

[14] Tan, M., Pang, R., Le, Q.V. (2020). EfficientDet: Scalable and efficient object detection. In *2020 IEEE/CVF Conference on Computer Vision and Pattern Recognition (CVPR)*, Seattle, WA, USA, pp. 10778-10787. <https://doi.org/10.1109/CVPR42600.2020.01079>

[15] Taigman, Y., Yang, M., Ranzato, M.A., Wolf, L. (201). DeepFace: Closing the gap to human-level performance in face verification. In *2014 IEEE Conference on*

- Computer Vision and Pattern Recognition, Columbus, OH, USA, pp. 1701-1708. <https://doi.org/10.1109/CVPR.2014.220>
- [16] Deng, J., Guo, J., Xue, N., Zafeiriou, S. (2019). Arcface: Additive angular margin loss for deep face recognition. In Proceedings of the IEEE/CVF Conference on Computer Vision and Pattern Recognition, Beach, CA, USA, pp. 4690-4699. <https://doi.org/10.1109/CVPR.2019.00482>
- [17] Lim, Y.S., Lee, S.H., Cheong, S.J., Park, Y.H. (2023). A long-distance 3D face recognition architecture utilizing MEMS-based region-scanning LiDAR. *MOEMS and Miniaturized Systems XXII*, 12434: 87-91. <https://doi.org/10.1117/12.2649500>
- [18] Niu, W., Zhao, Y., Yu, Z., Liu, Y., Gong, Y. (2023). Research on a face recognition algorithm based on 3D face data and 2D face image matching. *Journal of Visual Communication and Image Representation*, 91: 103757. <https://doi.org/10.1016/j.jvcir.2023.103757>
- [19] Hsieh, C.F., Liu, P.H., Lai, J.X., Sun, S.H. (2022). Implementation of a smart checkout system based on face recognition using YOLO v3-tiny. In 2022 IEEE 11th Global Conference on Consumer Electronics (GCCE), Osaka, Japan, pp. 903-904. <https://doi.org/10.1109/GCCE56475.2022.10014330>
- [20] Toshev, A., Szegedy, C. (2014). Deeppose: Human pose estimation via deep neural networks. In Proceedings of the IEEE Conference on Computer Vision and Pattern Recognition, Columbus, OH, USA, pp. 1653-1660. <https://doi.org/10.1109/CVPR.2014.214>
- [21] Chen, Y.C., Huang, Z.K., Pang, L., Jiang-Lin, J.Y., Kuo, C.H., Shuai, H.H., Cheng, W.H. (2023). Seeing the unseen: Wifi-based 2D human pose estimation via an evolving attentive spatial-Frequency network. *Pattern Recognition Letters*, 171: 21-27. <https://doi.org/10.1016/j.patrec.2023.04.020>
- [22] Yang, H., Jia, J., Lu, X. (2023). A multilevel object pose estimation algorithm based on point cloud keypoints. *Applied Intelligence*, 53: 18508-18516. <https://doi.org/10.1007/s10489-022-04411-5>
- [23] Yang, W., Ouyang, W., Wang, X., Ren, J., Li, H., Wang, X. (2018). 3D human pose estimation in the wild by adversarial learning. In 2018 IEEE/CVF Conference on Computer Vision and Pattern Recognition, Lake City, UT, USA, pp. 5255-5264. <https://doi.org/10.1109/CVPR.2018.00551>
- [24] Zhang, X., Chen, Z., Gao, J., Huang, W., Li, P., Zhang, J. (2022). A two-stage deep transfer learning model and its application for medical image processing in Traditional Chinese Medicine. *Knowledge-Based Systems*, 239: 108060. <https://doi.org/10.1016/j.knosys.2021.108060>
- [25] Kim, S.B., Kim, J.Y., Park, S.W., Lee, N.R., Kim, Y.H., Lee, K.J., Lee, Y.H. (2012). Effects of PEMFs (pulsed electromagnetic fields) stimulation on acupoint in quadriceps fatigue recovery. *International Journal of Precision Engineering and Manufacturing*, 13: 1697-1703. <https://doi.org/10.1007/s12541-012-0222-0>
- [26] Simonyan, K., Zisserman, A. (2014). Very deep convolutional networks for large-scale image recognition. arXiv preprint arXiv:1409.1556.
- [27] Wang, Q., Du, J., Wu, H. X., Pan, J., Ma, F., Lee, C. H. (2023). A four-stage data augmentation approach to ResNet-Conformer based acoustic modeling for sound event localization and detection. *IEEE/ACM Transactions on Audio, Speech, and Language Processing*, 31: 1251-1264. <https://doi.org/10.1109/TASLP.2023.3256088>
- [28] Sharif Razavian, A., Azizpour, H., Sullivan, J., Carlsson, S. (2014). CNN features off-the-shelf: An astounding baseline for recognition. In Proceedings of the IEEE Conference on Computer Vision and Pattern Recognition Workshops, Columbus, OH, USA, pp. 806-813. <https://doi.org/10.1109/CVPRW.2014.131>